Letter

Ultrafast nonequilibrium dynamics and high-harmonic generation in two-dimensional quantum spin Hall materials

Rajesh K. Malla,[1,2,3] Dasol Kim,[4,5] Dong Eon Kim,[4,5] Alexis Chacón,[4,5] and Wilton J. M. Kort-Kamp[1,*]

[1]*Theoretical Division, Los Alamos National Laboratory, Los Alamos, New Mexico 87545, USA*
[2]*Center for Nonlinear Studies, Los Alamos National Laboratory, Los Alamos, New Mexico 87545, USA*
[3]*Condensed Matter Physics and Materials Science Division, Brookhaven National Laboratory, Upton, New York 11973, USA*
[4]*Department of Physics and Center for Attosecond Science and Technology, POSTECH, 7 Pohang 37673, South Korea*
[5]*Max Planck POSTECH/KOREA Research Initiative, Pohang 37673, South Korea*

(Received 26 July 2022; revised 11 January 2023; accepted 26 April 2023; published 15 May 2023)

We develop the theoretical framework of nonequilibrium ultrafast photonics in monolayer quantum spin Hall insulators supporting a multitude of topological states. In these materials, ubiquitous strong light-matter interactions in the femtosecond scale lead to nonadiabatic quantum dynamics, resulting in topology-dependent nonlinear optoelectronic transport phenomena. We investigate the mechanism driving topological Dirac fermions interacting with strong ultrashort light pulses and uncover various experimentally accessible physical quantities that encode fingerprints of the quantum material's topological electronic state from the high-harmonic generated spectrum. Our work sets the theoretical cornerstones to realize the full potential of time-resolved harmonic spectroscopy for understanding nonequilibrium processes in quantum topological systems and identifying topological invariants in two-dimensional quantum spin Hall solid state systems.

DOI: 10.1103/PhysRevMaterials.7.L051201

Two-dimensional (2D) quantum spin Hall insulators (QSHIs) are atomically thin materials that support counter-propagating helical metallic spin edge states with zero net electronic conductance [1–5]. This quantum state of matter is protected by time-reversal symmetry and the robustness of its chiral spin currents against disorder, perturbations, and dissipation could serve as a route for coherent information transport across the nodes of quantum networks, enabling new technologies in quantum information science [6,7]. Kane and Mele suggested that spin-orbit coupling (SOC) in 2D materials produce a gap in the energy band structure that ultimately results in a QSHI state [8,9]. Although the exfoliation of graphene [10] paved the way for demonstrating various Hall effects in monolayers [11–18], the realization of QSHI states in graphene remains elusive due to its minimal SOC [19]. Various other 2D materials with stronger SOC [20–22] that can serve as QSHIs have been proposed, such as antiferromagnetic manganese chalcogenophosphates [23] and perovskites [24], and realized experimentally, including silicene [25], germanene [26], stanene [27], and plumbene [28], and recently developed jacutingaite materials [29–32]. These systems support topological phases that can be controlled via external interactions and fields [33–41], providing an all-in-one material platform for on-demand multioptoelectronic functionalities.

Nonlinear optical spectroscopy has been a go-to method to probe quantum systems with discrete energy levels, e.g., in atomic and molecular systems [42–47]. It has also been extended to solid-state systems, in which case an intense laser excites charge carriers to highly nonequilibrium states and the corresponding spectra, resulting from high-harmonic generation (HHG), serves as a tool to examine material properties [48–55]. Single-atomic-layer solids have become an attractive platform to elucidate the underlying mechanisms governing HHG since they do not suffer from phase-matching condition effects [56–61]. Recently, it has been proposed that ultrafast spectroscopy could be used to study chiral Hall states of quantum materials [62–65]. It has been shown that subgap harmonic generation is significantly enhanced in topological phases of finite-size one-dimensional chains of nanoparticles [66–68] and Haldane nanoribbons [69]. Moreover, circular dichroism and helicity of the emitted harmonics could be employed for sensing the topology of the electronic band structure of 2D Chern insulators [70–72]. Furthermore, noninteger HHG from surface states in three-dimensional bismuth-telluride insulators has been observed [73].

Prior works on 2D QSHIs have investigated their interaction with low-intensity monochromatic plane waves [33–41]. These studies consider only the weak-field regime and are limited to the linear regime or the leading nonlinear harmonic. Experimentally, more attractive strong-field dynamics in 2D QSHIs interacting with high-intensity ultrafast light pulses, thus leading to HHG and nonlinear signatures in the time domain, remains uncharted to date. Here, we bridge this knowledge gap by developing the theoretical cornerstones of the nonequilibrium dynamics of Dirac-like fermions in 2D QSHIs and use it to study topological phase transition fingerprints in their ultrafast response. We unveil the physical mechanisms driving the hot-electron population in a multitude of topologically protected quantum states supported by these materials. We show that competing intraband and interband

*kortkamp@lanl.gov

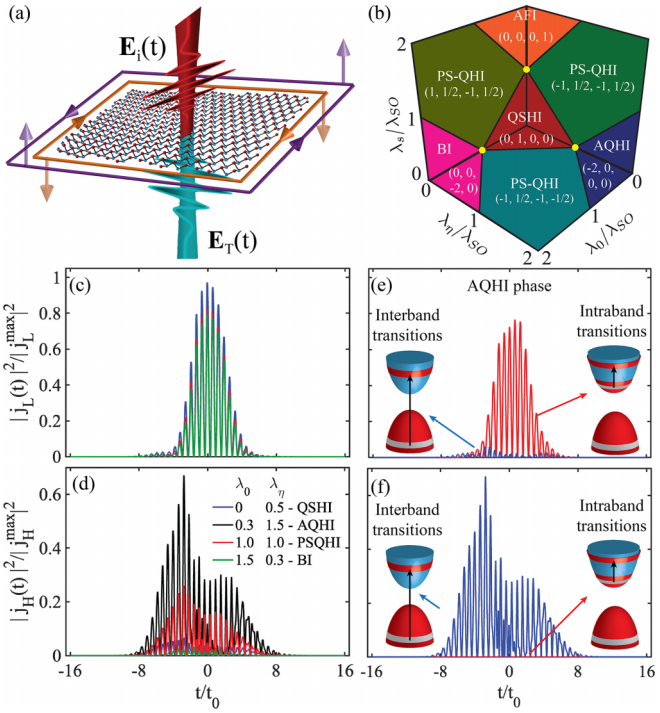

FIG. 1. (a) Strong-field physics in a Kane-Mele quantum spin Hall monolayer interacting with an ultrashort optical pulse. (b) Electronic phases supported by the system are the quantum spin Hall insulator (QSHI), anomalous quantum Hall insulator (AQHI), band insulator (BI), antiferromagnetic insulator (AFMI), and polarized-spin quantum Hall insulator (PS-QHI) [33–41]. Their Chern, spin Chern, valley Chern, and spin-valley Chern numbers are shown in parentheses. (c) Longitudinal and (d) Hall currents for selected phases. Contributions from intraband and interband transitions to $j_L(t)$ and $j_H(t)$ are shown in (e) and (f) for the AQHI phase. The parameters of the incident laser are $ev_F A_0/\lambda_{SO} = 5$, $\hbar\omega_0/\lambda_{SO} = 5$, and $\tau = 8t_0$, where $t_0 = \hbar/\lambda_{SO}$. We assume an electronic relaxation rate of $\hbar\Gamma/\lambda_{SO} = 0.05$ and an equilibrium Fermi energy $E_F = 0$.

transitions govern the trade-off between nonlinear Hall and longitudinal currents, leading to emerging ultrafast effects due to the backaction of charge carriers in the optical field. We also demonstrate nonadiabatic quantum electronic transport and discover various physical quantities, both in time and frequency domains, that serve as metrological probes of the energy band structure's topology in these materials.

We consider a generalized two-dimensional quantum spin Hall insulator interacting with an ultrashort optical pulse, as shown in Fig. 1(a). For concreteness, we assume that the energy band structured of the monolayer is described by a generalized Kane-Mele Hamiltonian $H_s^\eta(\mathbf{k}) = \hbar v_F(\eta k_x\tau_x + k_y\tau_y) + \Delta_s^\eta\tau_z$, which captures all the topological properties and dynamics of the full tight-binding model in the low-energy regime [36]. Here, $\mathbf{p} = \hbar\mathbf{k} = \hbar(k_x, k_y)$ is the particle momentum, v_F the Fermi velocity, τ_i the sublattice pseudospin Pauli matrices, and $\eta, s = \pm 1$ the valley and spin indices. The mass term $\Delta_s^\eta = \eta s\lambda_{SO} - \lambda_0 - \eta\lambda_\eta + s\lambda_s$ is the half energy band gap for a particular Dirac cone. It is determined by the intrinsic SOC λ_{SO} as well as by three knobs $\lambda_0, \lambda_\eta, \lambda_s$ representing interactions with external systems or fields. The λ_0 term describes, e.g., the staggered sublattice potential induced by a static electric field applied normal to a monolayer of the graphene family [33]. The λ_η component corresponds to a second-neighbor hopping that arises due to the coupling with a high-frequency off-resonant circularly polarized laser that induces an anomalous quantum Hall phase [34,74,75]. The λ_s term depicts the antiferromagnetic exchange interaction due to an interaction of the 2D material with a substrate [35]. On demand manipulation of λ_0, λ_η, and λ_s enables a wealth of topological phases and transitions, as shown in Fig. 1(b).

The impinging light drives the monolayer out of equilibrium and photoexcites a nonthermal free carrier density. Following electron relaxation and electron-hole recombination mechanisms leads to the emission of harmonics of the incident field, which encode signatures of the material's energy band structure. The transmitted optical pulse $\mathbf{E}_T(t)$ follows from Maxwell's equations subjected to boundary conditions at the monolayer, and at normal incidence $\mathbf{E}_T(t) = -\partial_t\boldsymbol{A}(t) - \mu_0 c\mathbf{j}(t)/2$, where $\boldsymbol{A}(t) = A_0 e^{-(4\log 2)t^2/\tau^2}\cos(\omega_0 t)\hat{\mathbf{x}}$ is the vector potential of the linearly polarized incident field. The total current can be explicitly expressed using longitudinal and Hall surface currents, denoted respectively by $j_L(t)$ and $j_H(t)$, as $\mathbf{j}(t) = j_L(t)\hat{\mathbf{x}} + j_H(t)\hat{\mathbf{y}}$. The quantum dynamics of 2D QSHIs and their topology footprints in the optical field via $\mathbf{j}(t)$ is obtained from the above Hamiltonian through a minimal fermion-light coupling substitution [76] $\hbar\boldsymbol{k} \to \boldsymbol{\Pi}_\mathbf{k}(t) = \boldsymbol{p} - e\boldsymbol{A}(t)$. The time dependence of the Hamiltonian through $\boldsymbol{A}(t)$ prevents analytical solutions to the Dirac equation beyond the weak-coupling regime [40,41]. Nonperturbative numerical results can be obtained by extending the formalism of Refs. [77,78] to massive topological fermions. It consists in writing the electronic spinor $|\psi_\mathbf{k}^{\eta,s}(t)\rangle$ as a linear combination of instantaneous eigenstates of $H_s^\eta[\boldsymbol{\Pi}_\mathbf{k}(t)]$, enabling one to derive coupled Dirac-Bloch differential equations for the population difference and interband coherence. These equations can be made SOC invariant by expressing all physical quantities in units of λ_{SO}, making their solutions and the ensuing electronic currents universal to any Kane-Mele QSHI monolayer [79].

We numerically solve the Dirac-Bloch equations to unveil the mechanisms governing the ultrafast dynamics of topological Dirac-like fermions in the monolayer. We focus our discussion to the $(\lambda_0, \lambda_\eta)$ plane, but similar conclusions hold for the entire phase diagram. Figures 1(c) and 1(d) show the temporal evolution of $j_L(t)$ and $j_H(t)$ for selected points in the phase diagram. The current components have a very distinct behavior due to the nature of the quantum transitions that drive each of them [see Figs. 1(e) and 1(f)]. Intraband transitions dominate $j_L(t)$ and lead to a longitudinal current nearly independent of the chosen electronic phase and quasisymmetric about the time $t = 0$, when the incident field reaches peak intensity. In contrast, the Hall current is strongly influenced by the choice of $(\lambda_0, \lambda_\eta)$ and its magnitude is enhanced in topological phases with nonzero Chern number $\mathcal{C}$ since $j_H(t)$ is largely governed by interband transitions. The Hall current is excited earlier in the ultrafast process, presents an asymmetric temporal response with respect to the center of the optical pulse, and has a longer duration than its longitudinal counterpart. This is because the weight of contributions from competing transitions varies as the strong field modulates the

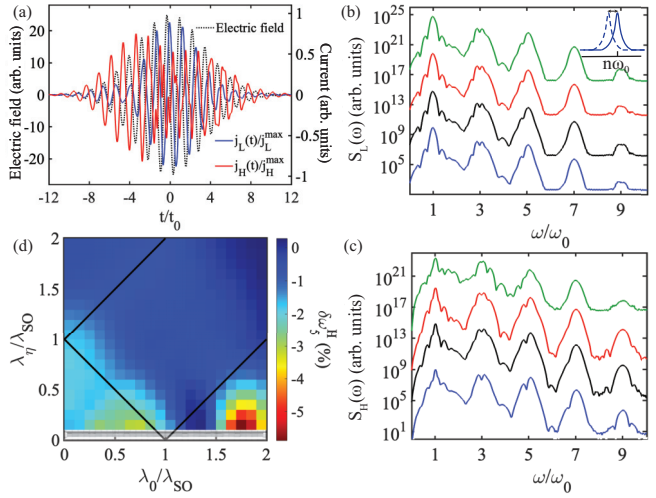

FIG. 2. (a) Comparison of $j_L(t)$ and $j_H(t)$ with the driving field highlights the nonadiabatic quantum dynamics and anharmonic evolution of the currents in the system for the AQHI phase. High-harmonic spectrum due to (b) $S_L(\omega)$ and (c) $S_H(\omega)$ for the same electronic phases in Fig. 1. For clear visualization we have vertically shifted (10^5 arb. units) the curves' baselines. The inset in (b) schematically shows the relative frequency shift $\delta\omega_n^{L,H}$ of each harmonic with respect to their nominal value $n\omega_0$ [79]. (d) Effects of the topological phase transitions in $\delta\omega_n^H$ for the fifth harmonic in the Hall field.

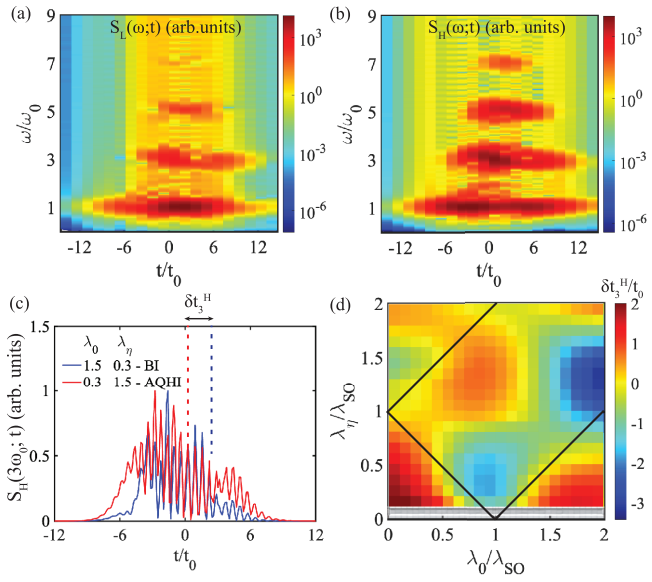

FIG. 3. Time-resolved harmonic emission. Gabor transform $S_L(\omega;t)$ and $S_H(\omega;t)$ of the (a) longitudinal and (b) Hall currents for the AQHI phase. (c) Dynamics of emission of the third harmonic for two energetically equivalent, but topologically distinct, points in the phase space: $(\lambda_0, \lambda_\eta, \lambda_s) = (0.3, 1.5, 0)$ and $(\lambda_0, \lambda_\eta, \lambda_s) = (1.5, 0.3, 0)$. (d) Phase diagram of the average time delay of emission [79] for the third harmonic for the Hall current.

hot-electron population, and we assume that the material is originally in thermal equilibrium with Fermi energy $E_F = 0$. Initially, only interband transitions are possible and lead to the early excitation of Hall currents. As the conduction band gets populated, interband transitions near the band gap become energetically forbidden while intraband transitions are enabled. This results in a small decrease in $j_H(t)$ and excitation of late longitudinal currents. Finally, as electron-hole pairs relax and recombine, low-energy interband transitions resume, leading to a second peak in the envelope of $j_H(t)$ before the interaction with the optical pulse vanishes. This complex dynamics in $j_L(t)$ and $j_H(t)$ is only possible due to the ultrafast and strongly nonlinear nature of the laser-monolayer interaction.

In Fig. 2 we investigate the backaction of the hot-electron population on the light pulse. Because the monolayer mass gaps are significantly smaller than the energy of the incident photons, the impinging pulse near instantaneously photogenerates free carriers. The carriers synchronously follow the electric field oscillations during the leading edge of the pulse [Fig. 2(a)] with the longitudinal (Hall) current in (out of) phase with the incident field. The excitation of electron-hole pairs occurs in a timescale faster than the duration of the optical pulse, which results in a switch from a semiconducting to a metal-like response with a time-dependent plasma frequency as the interaction evolves. Consequently, the trailing edge of the light pulse envelope probes a transient and rapidly changing electronic population. This causes nonadiabatic quantum evolution of the fermionic currents, which develop a temporal lag with respect to the driving field at later times in the interaction [Fig. 2(a)]. Figures 2(b) and 2(c) show that the anharmonic response of the monolayer results in odd-order HHG in the scattered field. We mention that the full tight-binding Hamiltonian of 2D QSHIs may include also higher-energy contributions that break spatial inversion symmetry, thus leading to some generation of even harmonics. For the parameters in our calculations we checked that even-order harmonics can be neglected. We can distinguish up to the ninth harmonic in the emission spectra $S_{L,H}(\omega) = |\omega j_{L,H}(\omega)|^2$, where $j_{L,H}(\omega)$ are the Fourier transforms of $j_{L,H}(t)$. HHG spectra for varying intensities of the incident laser are shown in the Supplemental Material [79]. Consistent with Figs. 2(c) and 2(d), the intensity $S_L(\omega)$ of each harmonic (unshifted baselines, not shown) is quasi-independent of the electronic phase of the system, while $S_H(\omega)$ is strongly phase dependent. Note that the shape of $S_H(\omega)$ corresponding to the QSHI and BI phases vary slightly from each other even though they have $\mathcal{C} = 0$. This is because the HHG intensity depends on both the energy landscape (magnitude of the gaps, $|\Delta_s^\eta|$) as well as the topology [sign of Dirac gaps, $\mathrm{sgn}(\Delta_s^\eta)$] of the band structure. Note also that 2D QSHIs emit harmonics at frequencies which are slightly shifted with respect to their nominal value [inset in Fig. 2(b)]. This shift has been reported for other materials [60,80,81], and may encode signatures of nonlinear dynamics in the system. In Fig. 2(d) we show that the underlying topological phase of two-dimensional QHSIs affects the relative frequency shift of $S_H(\omega)$, being enhanced (suppressed) in phases with $\mathcal{C} = 0$ ($\mathcal{C} \neq 0$).

In Figs. 3(a) and 3(b) we show the time-resolved emission spectrum of harmonics for a representative phase with a nonzero Chern number. The plots reveal that higher harmonics are more likely to be excited in $S_H(\omega)$ than in $S_L(\omega)$. They show that while the fundamental harmonic is continuously excited, HHG occurs at later times during the interaction. Our

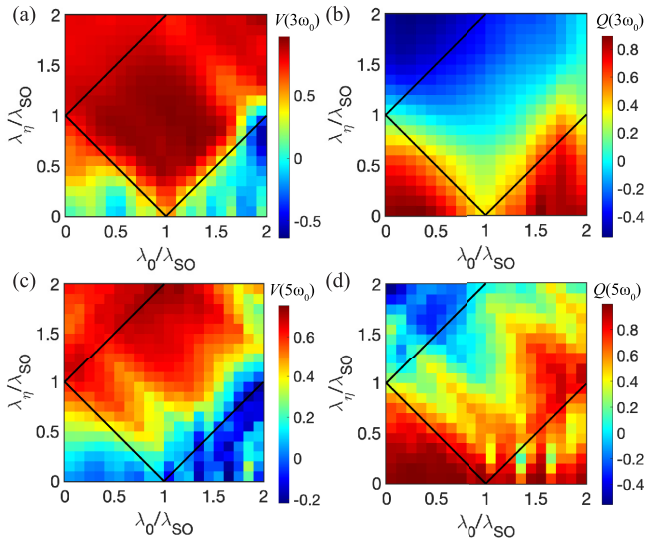

FIG. 4. Topology fingerprints in the polarization state. Phase diagram of the Stokes parameters (a), (c) V for circular and (b), (d) Q for linear polarization for the third (top) and fifth (bottom) harmonics.

results also demonstrate that the initial time of excitation of a harmonic and its duration scale inversely with the frequency of emission. Thus, HHG is generally confined to time intervals when the incident field approaches its maximum intensity and only lower-order harmonics appear near the leading and trailing edges of the optical pulse. Figure 3(c) reveals that quantum states in 2D QSHIs with contrasting topological properties lead to different temporal dynamics in the emission of each spectral component of the Hall current. We note that harmonics are emitted at later times for topologically trivial phases when compared with states with $\mathcal{C} \neq 0$. The time delay associated to the generation of a harmonic and its dependence on the topology of the monolayer can be quantified via the mean time of emission δt_n^H (see Supplemental Material [79]). Figure 3(d) shows that δt_3^H has a serendipitous dependence on the external parameters λ_0, λ_η. It evidences that the third harmonic is emitted with a delay with respect to the incident pulse peak power, with larger (smaller) temporal lags occurring for phases with $\mathcal{C} = 0$ ($\mathcal{C} \neq 0$). Similar results hold for other harmonics. This topology-dependent time delay in harmonic emission stems from the cross-coupling between the band structure's Berry curvature and the time-varying incident field, which offsets from the Dirac points K and K' the optimum momentum for valence-to-conduction band charge carrier injection, similar to the case of Chern insulators [70]. These findings indicate the potential of time-resolved harmonic spectroscopy for identifying topological invariants in solid state systems.

In Fig. 4 we investigate the polarization state of the emitted harmonics, which strongly depends on the intrinsic topology of the energy band structure via the coupling constants λ_0, λ_η, and λ_s. For concreteness we consider the normalized Stokes parameters $V = -2\,\mathrm{Im}[j_L(\omega) j_H^*(\omega)]/I$ and $Q = [|j_L(\omega)|^2 - |j_H(\omega)|^2]/I$, where $I = |j_L(\omega)|^2 + |j_H(\omega)|^2$ is the frequency-resolved intensity of the field. Note that V is also referred to in the literature as helicity and has been previously employed to distinguish between topologically trivial and nontrivial phases in the Haldane model via circular polarization harmonic emission [70–72], while Q represents the asymmetry between harmonics generated with linear polarization parallel to either the longitudinal or the Hall currents. Figure 4(a) shows that the Stokes parameter V varies significantly across various phase boundaries and clearly distinguishes phases with zero Chern and nonzero Chern numbers. The changes in V highlight that in topologically trivial (nontrivial) phases the state of the generated harmonics is primarily dominated by right (left) circular polarization. As evidenced by the phase diagram for the fifth harmonic shown in Fig. 4(c), this behavior of V is robust and holds for higher harmonics as well. Note, however, that V fails to differentiate between two nontrivial topological phases, e.g., the AQHI ($\mathcal{C} = -2$) and the PS-QHI ($\mathcal{C} = -1$) phases. This can be resolved by noticing that the Stokes parameter Q [Figs. 4(b) and 4(d)] not only separates topologically trivial and nontrivial electronic states, but it also enables one to distinguish between phases with nonzero Chern numbers. This is due to the increase of the nonlinear Hall current with the Chern number, enhancing the emission of high harmonics polarized orthogonally to the incident light. This provides a mechanism to investigate the topology of the monolayer beyond the linear response regime. The results in Figs. 4(b) and 4(d) suggest that Q is a suitable observable, of easy access experimentally, to quantify topological fingerprints in the HHG spectra.

We have developed a comprehensive theoretical and numerical framework for investigating topological phase transitions in monolayer topological quantum spin Hall materials via ultrafast nonlinear photonic processes. As a prototype example, we considered systems described via a generalized Kane-Mele Hamiltonian which includes a diversity of knobs that can be controlled externally to drive the system across a multitude of topological phase transitions. We unveiled the full dynamics of the 2D QSHIs when interacting with strong ultrashort light pulses and showed that various physical quantities can be used to identify and characterize the materials' electronic state. Recent progress in the synthesis of various topological semiconductors, e.g., graphene family monolayers and jacutingaite materials, together with advances in nonlinear characterization photonic techniques implies that our results can be accessed experimentally with current technologies. For example, measurement of Stokes parameters can be realized by employing commercially available polarizers. The frequency shift and time delay are ∼10–50 THz and ∼1–10 fs for the third harmonic when we consider an incident laser pulse with intensity 3000 GW/cm^2, $\omega_0/2\pi = 360$ THz, $\tau = 30$ fs, and a monolayer with $\lambda_{SO} = 0.3$ meV, all within existing measurement capabilities.

R.K.M. and W.J.M.K.-K. acknowledge the Laboratory Directed Research and Development program of Los Alamos National Laboratory under Project No. 20190574ECR. R.K.M. also thanks the Center for Nonlinear Studies at LANL for financial support under Project No. 20190495CR. In the later part of the project, R.K.M. was partially supported by the U.S. Department of Energy, Office of Science, Basic Energy Sciences, Materials Sciences and Engineering Division, Condensed Matter Theory Program at Brookhaven National Lab-

oratory. D.K. and A.C. are thankful for the support from the National Research Foundation of Korea (NRF) grants (Grants No. 2022M3H4A1A04074153, No. 2020R1A2C2103181, and No. RS-2022-00154676) funded by the Ministry of Science, ICT, and from Korea Institute for Advancement of Technology (KIAT) grant funded by the Korea Government (MOTIE) (P0008763, HRD Program for Industrial Innovation).

[1] B. A. Bernevig, T. L. Hughes, and S.-C. Zhang, Quantum spin Hall effect and topological phase transition in HgTe quantum wells, Science **314**, 1757 (2006).

[2] M. König, S. Wiedmann, C. Brüne, A. Roth, H. Buhmann, L. W. Molenkamp, X.-L. Qi, and S.-C. Zhang, Quantum spin Hall insulator state in HgTe quantum wells, Science **318**, 766 (2007).

[3] A. Roth, C. Brüne, H. Buhmann, L. W. Molenkamp, J. Maciejko, X.-L. Qi, and S.-C. Zhang, Nonlocal transport in the quantum spin Hall state, Science **325**, 294 (2009).

[4] M. Z. Hasan and C. L. Kane, Colloquium: Topological insulators, Rev. Mod. Phys. **82**, 3045 (2010).

[5] C. Brüne, A. Roth, H. Buhmann, E. Hankiewicz, L. W. Molenkamp, J. Maciejko, X.-L. Qi, and S.-C. Zhang, Spin polarization of the quantum spin Hall edge states, Nat. Phys. **8**, 485 (2012).

[6] A. Manchon, H. C. Koo, J. Nitta, S. M. Frolov, and R. A. Duine, New perspectives for Rashba spin-orbit coupling, Nat. Mater. **14**, 871 (2015).

[7] Y. Tokura, M. Kawasaki, and N. Nagaosa, Emergent functions of quantum materials, Nat. Phys. **13**, 1056 (2017).

[8] C. L. Kane and E. J. Mele, Quantum Spin Hall Effect in Graphene, Phys. Rev. Lett. **95**, 226801 (2005).

[9] C. L. Kane and E. J. Mele, Z_2 Topological Order and the Quantum Spin Hall Effect, Phys. Rev. Lett. **95**, 146802 (2005).

[10] K. S. Novoselov, A. K. Geim, S. V. Morozov, D. Jiang, Y. Zhang, S. V. Dubonos, I. V. Grigorieva, and A. A. Firsov, Electric field effect in atomically thin carbon films, Science **306**, 666 (2004).

[11] Y. Zhang, Y.-W. Tan, H. L. Stormer, and P. Kim, Experimental observation of the quantum Hall effect and Berry's phase in graphene, Nature (London) **438**, 201 (2005).

[12] V. P. Gusynin and S. G. Sharapov, Unconventional Integer Quantum Hall Effect in Graphene, Phys. Rev. Lett. **95**, 146801 (2005).

[13] K. S. Novoselov, Z. Jiang, Y. Zhang, S. V. Morozov, H. L. Stormer, U. Zeitler, J. C. Maan, G. S. Boebinger, P. Kim, and A. K. Geim, Room-temperature quantum Hall effect in graphene, Science **315**, 1379 (2007).

[14] K. I. Bolotin, F. Ghahari, M. D. Shulman, H. L. Stormer, and P. Kim, Observation of the fractional quantum Hall effect in graphene, Nature (London) **462**, 196 (2009).

[15] G. Guinea, M. Katsnelson, and A. K. Geim, Energy gaps and a zero-field quantum Hall effect in graphene by strain engineering, Nat. Phys. **6**, 30 (2010).

[16] N. Levy, S. A. Burke, K. L. Meaker, M. Panlasigui, A. Zettl, F. Guinea, A. H. Castro Neto, and M. F. Crommie, Strain-induced pseudo–magnetic fields greater than 300 tesla in graphene nanobubbles, Science **329**, 544 (2010).

[17] Y. Jiang, J. Mao, J. Duan, X. Lai, K. Watanabe, T. Taniguchi, and E. Y. Andrei, Visualizing strain-induced pseudomagnetic fields in graphene through an hBN magnifying glass, Nano Lett. **17**, 2839 (2017).

[18] M. Schmitz, T. Ouaj, Z. Winter, K. Rubi, K. Watanabe, T. Taniguchi, U. Zeitler, B. Beschoten, and C. Stampfer, Fractional quantum Hall effect in CVD-grown graphene, Fractional quantum Hall effect in CVD-grown graphene, 2D Mater. **7**, 041007 (2020).

[19] S. Konschuh, M. Gmitra, and J. Fabian, Tight-binding theory of the spin-orbit coupling in graphene, Phys. Rev. B **82**, 245412 (2010).

[20] A. Castellanos-Gomez, Why all the fuss about 2D semiconductors? Nat. Photonics **10**, 202 (2016).

[21] A. Molle, J. Goldberger, M. Houssa, Y. Xu, S.-C. Zhang, and D. Akinwande, Buckled two-dimensional Xene sheets, Nat. Mater. **16**, 163 (2017).

[22] A. J. Mannix, B. Kiraly, M. C. Hersam, and N. P. Guisinger, Synthesis and chemistry of elemental 2D materials, Nat. Rev. Chem. **1**, 0014 (2020).

[23] X. Li, T. Cao, Q. Niu, J. Shi, and J. Feng, Coupling the valley degree of freedom to antiferromagnetic order, Proc. Natl. Acad. Sci. USA **110**, 3738 (2013).

[24] Q.-F. Liang, L.-H. Wu, and X. Hu, Electrically tunable topological state in [111] perovskite materials with an antiferromagnetic exchange field, New J. Phys. **15**, 063031 (2013).

[25] P. Vogt, P. DePadova, C. Quaresima, J. Avila, E. Frantzeskakis, M. C. Asensio, A. Resta, B. Ealet, and G. Le Lay, Silicene: Compelling Experimental Evidence for Graphenelike Two-Dimensional Silicon, Phys. Rev. Lett. **108**, 155501 (2012).

[26] M. E. Dávila, L. Xian, S. Cahangirov, A. Rubio, and G. L. Lay, Germanene: a novel two-dimensional germanium allotrope akin to graphene and silicene, New J. Phys. **16**, 095002 (2014).

[27] F.-F. Zhu, W.-J. Chen, Y. Xu, C.-l. Gao, D.-d. Guan, C.-H. Liu, D. Qian, S.-C. Zhang, and J.-F. Jia, Epitaxial growth of two-dimensional stanene, Nat. Mater. **14**, 1020 (2015).

[28] J. Yuhara, B. He, N. Matsunami, M. Nakatake, and G. Le Lay, Graphene's latest cousin: Plumbene epitaxial growth on a "Nano WaterCube", Adv. Mater. **31**, 1901017 (2019).

[29] A. Marrazzo, M. Gibertini, D. Campi, N. Mounet, and N. Marzari, Prediction of a Large-Gap and Switchable Kane-Mele Quantum Spin Hall Insulator, Phys. Rev. Lett. **120**, 117701 (2018).

[30] A. Marrazzo, M. Gibertini, D. Campi, N. Mounet, and N. Marzari, Relative abundance of Z_2 topological order in exfoliable two-dimensional insulators, Nano Lett. **19**, 8431 (2019).

[31] A. Marrazzo, N. Marzari, and M. Gibertini, Emergent dual topology in the three-dimensional Kane-Mele Pt_2HgSe_3, Phys. Rev. Res. **2**, 012063(R) (2020).

[32] I. Cucchi, A. Marrazzo, E. Cappelli, S. Riccò, F. Y. Bruno, S. Lisi, M. Hoesch, T. K. Kim, C. Cacho, C. Besnard, E. Giannini, N. Marzari, M. Gibertini, F. Baumberger, and A. Tamai, Bulk and Surface Electronic Structure of the Dual-Topology Semimetal Pt_2HgSe_3, Phys. Rev. Lett. **124**, 106402 (2020).

[33] L. Stille, C. J. Tabert, and E. J. Nicol, Optical signatures of the tunable band gap and valley-spin coupling in silicene, Phys. Rev. B **86**, 195405 (2012).
[34] M. Ezawa, Photoinduced Topological Phase Transition and a Single Dirac-Cone State in Silicene, Phys. Rev. Lett. **110**, 026603 (2013).
[35] M. Ezawa, Spin valleytronics in silicene: Quantum spin Hall–quantum anomalous Hall insulators and single-valley semimetals, Phys. Rev. B **87**, 155415 (2013).
[36] M. Ezawa, Monolayer topological insulators: Silicene, germanene, and stanene, J. Phys. Soc. Jpn. **84**, 121003 (2015).
[37] P. Rodriguez-Lopez, W. J. M. Kort-Kamp, D. Dalvit, and L. M. Woods, Casimir force phase transitions in the graphene family, Nat. Commun. **8**, 14699 (2017).
[38] W. J. M. Kort-Kamp, Topological Phase Transitions in the Photonic Spin Hall Effect, Phys. Rev. Lett. **119**, 147401 (2017).
[39] P. Rodriguez-Lopez, W. J. M. Kort-Kamp, D. A. R. Dalvit, and L. M. Woods, Nonlocal optical response in topological phase transitions in the graphene family, Phys. Rev. Mater. **2**, 014003 (2018).
[40] R. K. Malla and W. J. M. Kort-Kamp, Nonlinear dynamics of topological Dirac fermions in 2D spin-orbit coupled materials, Sci. Rep. **11**, 9734 (2021).
[41] R. K. Malla, A. Saxena, and W. J. M. Kort-Kamp, Emerging nonlinear Hall effect in Kane-Mele two-dimensional topological insulators, Phys. Rev. B **104**, 205422 (2021).
[42] S. Baker, J. S. Robinson, C. A. Haworth, H. Teng, R. A. Smith, C. Chirila, C. M. Lein, J. W. G. Tisch, and J. P. Marangos, Probing proton dynamics in molecules on an attosecond time scale, Science **312**, 424 (2006).
[43] P. B. Corkum and F. Krausz, Attosecond, femtosecond, high harmonic generation, photoionisation, transient absorption, Nat. Phys. **3**, 381 (2007).
[44] F. Krausz and M. Ivanov, Attosecond physics, Rev. Mod. Phys. **81**, 163 (2009).
[45] D. Shafir, H. Soifer, B. D. Bruner, M. Dagan, Y. Mairesse, S. Patchkovskii, M. Y. Ivanov, O. Smirnova, and N. Dudovich, Resolving the time when an electron exits a tunnelling barrier, Nature (London) **485**, 343 (2012).
[46] F. Lépine, M. Y. Ivanov, and M. J. J. Vrakking, Attosecond molecular dynamics: Fact or fiction? Nat. Photonics **8**, 195 (2014).
[47] P. Peng, C. Marceau, and D. M. Villeneuve, Attosecond imaging of molecules using high harmonic spectroscopy, Nat. Rev. Phys. **1**, 144 (2019).
[48] M. F. Ciappina, J. A. Pérez-Hernández, A. S. Landsman, W. A. Okell, S. Zherebtsov, B. Förg, J. Schötz, L. Seiffert, T. Fennel, T. Shaaran, T. Zimmermann, A. Chacón, R. Guichard, A. Zaïr, J. W. G. Tisch, J. P. Marangos, T. Witting, A. Braun, S. A. Maier, L. Roso *et al.*, Attosecond physics at the nanoscale, Rep. Prog. Phys. **80**, 054401 (2017).
[49] D. N. Basov, R. D. Averitt, and D. Hsieh, Towards properties on demand in quantum materials, Nat. Mater. **16**, 1077 (2017).
[50] H. Liu, Y. Li, Y. S. You, S. Ghimire, T. F. Heinz, and D. A. Reis, High-harmonic generation from an atomically thin semiconductor, Nat. Phys. **13**, 262 (2017).
[51] Y. S. You, Y. Yin, A. Chew, X. Ren, S. Gholam-Mirzaei, and M. Chini, High-harmonic generation in amorphous solids, Nat. Commun. **8**, 724 (2018).
[52] S. Ghimire and D. A. Reis, High-harmonic generation from solids, Nat. Phys. **15**, 10 (2019).
[53] G. Vampa, H. Liu, T. F. Heinz, and D. A. Reis, Disentangling interface and bulk contributions to high-harmonic emission from solids, Optica **6**, 553 (2019).
[54] S. Kovalev, R. M. A. Dantas, S. Germanskiy, J.-C. Deinert, B. Green, I. Ilyakov, N. Awari, M. Chen, M. Bawatna, J. Ling, F. Xiu, P. H. M. van Loosdrecht, P. Surówka, T. Oka, and Z. Wang, Non-perturbative terahertz high-harmonic generation in the three-dimensional Dirac semimetal Cd_3As_2, Nat. Commun. **11**, 2451 (2020).
[55] M. Lysne, Y. Murakami, M. Schüler, and P. Werner, High-harmonic generation in spin-orbit coupled systems, Phys. Rev. B **102**, 081121(R) (2020).
[56] I. Gierz, J. C. Petersen, M. Mitrano, C. Cacho, I. C. E. Turcu, E. Springate, A. Stöhr, A. Köhler, U. Starke, and A. Cavalleri, Snapshots of non-equilibrium Dirac carrier distributions in graphene, Nat. Mater. **12**, 1119 (2013).
[57] N. Yoshikawa, T. Tamaya, and K. Tanaka, High-harmonic generation in graphene enhanced by elliptically polarized light excitation, Science **356**, 736 (2017).
[58] H. A. Hafez, S. Kovalev, J.-C. Deinert, Z. Mics, B. Green, N. Awari, M. Chen, S. Germanskiy, U. Lehnert, J. Teichert, Z. Wang, K.-J. Tielrooij, Z. Liu, Z. Chen, A. Narita, K. Müllen, M. Bonn, M. Gensch, and D. Turchinovich, Extremely efficient terahertz high-harmonic generation in graphene by hot Dirac fermions, Nature (London) **561**, 507 (2018).
[59] G. P. Zhang, M. S. Si, M. Murakami, Y. H. Bai, and T. F. George, Generating high-order optical and spin harmonics from ferromagnetic monolayers, Nat. Commun. **9**, 3031 (2018).
[60] M. Baudisch, A. Marini, J. D. Cox, T. Zhu, F. Silva, S. Teichmann, M. Massicotte, F. Koppens, L. S. Levitov, F. J. García de Abajo, and J. Biegert, Ultrafast nonlinear optical response of Dirac fermions in graphene, Nat. Commun. **9**, 1018 (2018).
[61] H. A. Hafez, S. Kovalev, K. J. Tielrooij, M. Bonn, M. Gensch, and D. Turchinovich, Terahertz nonlinear optics of graphene: From saturable absorption to high-harmonics generation, Adv. Opt. Mater. **8**, 1900771 (2020).
[62] T. Morimoto and N. Nagaosa, Topological nature of nonlinear optical effects in solids, Sci. Adv. **2**, e1501524 (2016).
[63] J. Reimann, S. Schlauderer, C. P. Schmid, F. Langer, S. Baierl, K. A. Kokh, O. E. Tereshchenko, A. Kimura, C. Lange, J. Güdde, U. Höfer, and R. Huber, Subcycle observation of lightwave-driven Dirac currents in a topological surface band, Nature (London) **562**, 396 (2018).
[64] T. T. Luu and H. J. Wörner, Measurement of the Berry curvature of solids using high-harmonic spectroscopy, Nat. Commun. **9**, 916 (2018).
[65] H. K. Avetissian, A. K. Avetissian, B. R. Avchyan, and G. F. Mkrtchian, Multiphoton excitation and high-harmonics generation in topological insulator, J. Phys.: Condens. Matter **30**, 185302 (2018).
[66] D. Bauer and K. K. Hansen, High-Harmonic Generation in Solids with and without Topological Edge States, Phys. Rev. Lett. **120**, 177401 (2018).
[67] C. Jürß and D. Bauer, High-harmonic generation in Su-Schrieffer-Heeger chains, Phys. Rev. B **99**, 195428 (2019).

[68] H. Drüeke and D. Bauer, Robustness of topologically sensitive harmonic generation in laser-driven linear chains, Phys. Rev. A **99**, 053402 (2019).

[69] C. Jürß and D. Bauer, Helicity flip of high-order harmonic photons in Haldane nanoribbons, Phys. Rev. A **102**, 043105 (2020).

[70] R. Silva, A. Jiménez-Galán, B. Amorim, O. Smirnova, and M. Ivanov, Topological strong-field physics on sub-laser-cycle timescale, Nat. Photonics **13**, 849 (2019).

[71] A. Chacón, W. Zhu, S. P. Kelly, A. Dauphin, E. Pisanty, A. Picón, C. Ticknor, M. F. Ciappina, A. Saxena, and M. Lewenstein, Circular dichroism in higher-order harmonic generation: Heralding topological phases and transitions in Chern insulators, Phys. Rev. B **102**, 134115 (2020).

[72] D. Baykusheva, A. Chacón, D. Kim, D. E. Kim, D. A. Reis, and S. Ghimire, Strong-field physics in three-dimensional topological insulators, Phys. Rev. A **103**, 023101 (2021).

[73] C. P. Schmid, L. Weigl, P. Grössing, V. Junk, C. Gorini, S. Schlauderer, S. Ito, M. Meierhofer, N. Hofmann, D. Afanasiev *et al.*, Tunable non-integer high-harmonic generation in a topological insulator, Nature (London) **593**, 385 (2021).

[74] T. Oka and H. Aoki, Photovoltaic Hall effect in graphene, Phys. Rev. B **79**, 081406(R) (2009).

[75] J. W. McIver, B. Schulte, F.-U. Stein, T. Matsuyama, G. Jotzu, G. Meier, and A. Cavalleri, Light-induced anomalous Hall effect in graphene, Nat. Phys. **16**, 38 (2020).

[76] J. E. Sipe and E. Ghahramani, Nonlinear optical response of semiconductors in the independent-particle approximation, Phys. Rev. B **48**, 11705 (1993).

[77] K. L. Ishikawa, Nonlinear optical response of graphene in time domain, Phys. Rev. B **82**, 201402(R) (2010).

[78] K. L. Ishikawa, Electronic response of graphene to an ultrashort intense terahertz radiation pulse, New J. Phys. **15**, 055021 (2013).

[79] See Supplemental Material at http://link.aps.org/supplemental/10.1103/PhysRevMaterials.7.L051201 for the derivation of ultrafast current and universal Dirac-Bloch equations in two-dimensional QSHI materials. Additional details regarding numerical evaluation and the high-harmonic generation dependence on laser intensity are also provided.

[80] S. Roy, A. Marini, and F. Biancalana, Self-frequency blueshift of dissipative solitons in silicon-based waveguide, Phys. Rev. A **87**, 065803 (2013).

[81] A. Blanco-Redondo, D. Eades, J. Li, S. Lefrancois, T. F. Krauss, B. J. Eggleton, and C. Husko, Controlling free-carrier temporal effects in silicon by dispersion engineering, Optica **1**, 299 (2014).